AIP | Review of Scientific Instruments

Determination of flux ionization fraction using a quartz crystal microbalance and a gridded energy analyzer in an ionized magnetron sputtering system

K. M. Green, D. B. Hayden, D. R. Juliano, and D. N. Ruzic

Citation: Rev. Sci. Instrum. **68**, 4555 (1997); doi: 10.1063/1.1148430
View online: http://dx.doi.org/10.1063/1.1148430
View Table of Contents: http://rsi.aip.org/resource/1/RSINAK/v68/i12
Published by the American Institute of Physics.

Related Articles

On the density of states of germanium telluride
J. Appl. Phys. 112, 113714 (2012)

Integration of high-dielectric constant Ta2O5 oxides on diamond for power devices
Appl. Phys. Lett. 101, 232907 (2012)

Intermixing of InGaAs/GaAs quantum wells and quantum dots using sputter-deposited silicon oxynitride capping layers
J. Appl. Phys. 112, 113511 (2012)

Improvement of (004) texturing by slow growth of Nd doped TiO2 films
J. Appl. Phys. 112, 113505 (2012)

Electrical and optical properties of Ta-Si-N thin films deposited by reactive magnetron sputtering
J. Appl. Phys. 112, 114302 (2012)

Additional information on Rev. Sci. Instrum.

Journal Homepage: http://rsi.aip.org
Journal Information: http://rsi.aip.org/about/about_the_journal
Top downloads: http://rsi.aip.org/features/most_downloaded
Information for Authors: http://rsi.aip.org/authors

ADVERTISEMENT

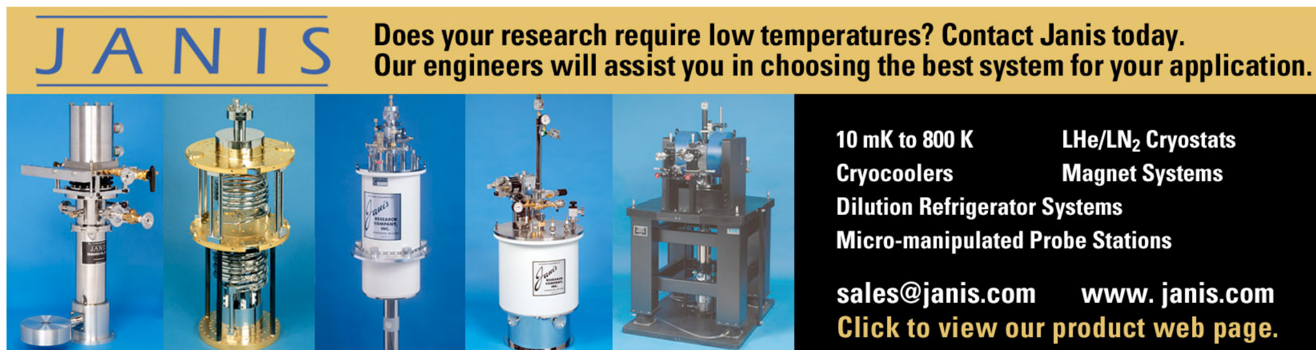

Downloaded 13 Dec 2012 to 130.126.32.13. Redistribution subject to AIP license or copyright; see http://rsi.aip.org/about/rights_and_permissions

Determination of flux ionization fraction using a quartz crystal microbalance and a gridded energy analyzer in an ionized magnetron sputtering system

K. M. Green, D. B. Hayden, D. R. Juliano, and D. N. Ruzic
University of Illinois, 103 South Goodwin Avenue, Urbana, Illinois 61801

(Received 4 March 1997; accepted for publication 21 August 1997)

A diagnostic which combines a quartz crystal microbalance (QCM) and a gridded energy analyzer has been developed to measure the metal flux ionization fraction in a modified commercial dc magnetron sputtering device. The sensor is mounted on a linear motion feedthrough and embedded in a slot in the substrate plane to allow for measuring the uniformity in deposition and ionization throughout the plane of the wafer. Radio-frequency (rf) power is introduced through a coil to ionize the Al atoms. The metal flux ionization fraction at the QCM is determined by comparing the total deposition rate with and without a bias that screens out the ions, but that leaves the plasma undisturbed. By varying the voltage applied to the grids, the plasma potential is determined. At a pressure of 35 mTorr, a magnetron power of 2 kW, and a net rf power of 310±5 W, 78±5% ionization was found. © *1997 American Institute of Physics.* [S0034-6748(97)03412-6]

I. INTRODUCTION

Chemical vapor deposition (CVD) and physical vapor deposition (PVD) are useful techniques for metallization of semiconductor wafers. CVD is adept in producing high purity thin films of near perfect crystalline structures for many materials.[1] However, in depositing aluminum, CVD fails to fill the entire volume of the trench or via.[2] The standard PVD techniques for depositing metal, sputtering and evaporation, can fill entire volumes of trenches or vias but do not provide good step coverage for high aspect-ratio (AR) trenches and vias when depositing aluminum.[2]

For conventional sputtering, the current trench-width limit for achieving good step coverage is 0.5 μm. The next generation of computer chips, however, requires the metallization of sub-half-micron features.[3]

With conventional sputtering techniques, the Al flux that reaches the substrate consists mainly of neutral atoms. These atoms arrive at the substrate surface at a variety of incident angles leading to pinchoff of the feature and void formation.

In trying to make sputtering a viable mechanism for filling high aspect ratio trenches, several techniques have been investigated including collimated sputtering and ionized sputtering. Collimated sputtering consists of using a physical filter located between the target and the substrate.[4] Rossnagel *et al.* have filled trenches with AR=3 using the collimated sputtering technique. Collimated sputtering does, however, have some drawbacks. The overall sputter flux from the target is decreased by the presence of the collimator. This series of tubes attenuates a great deal of the sputter flux because only atoms traveling within ±5° of normal incidence to the substrate will pass through the collimator. Also after several hours of operation, the collimators begin to clog decreasing still further the flux on the substrate. Additionally, the deposition that builds up on the sides of the collimator tends to flake off.[4]

Ionized sputtering achieves a directional flux by ionizing the metal atoms which are sputtered from the target. Then by applying a bias to the substrate, the metal ions are accelerated straight down into the trenches and vias at an energy equal to the charge times the difference between the plasma potential and the substrate bias. The particles that reach the substrate consist of directed ions and isotropic neutrals,[5] and can fill the narrow trenches needed on future chips. To evaluate potential ionized PVD apparatuses, a diagnostic that can measure the ionization fraction of the metal in the plasma or reaching the substrate is essential in determining the effectiveness of the ionization source.

A variety of methods to increase and measure the metal ionization fraction in a plasma have been used. Holber *et al.*[6] have achieved a completely ionized flux of Cu using a microwave source to excite Cu neutrals introduced into the vacuum chamber. A unique feature of their system is that the plasma incident on the substrate consists only of Cu ions and no other gas is present.

An experiment by Yamashita[7] uses a control mesh grid which is biased to repel or admit metal ions. These experiments are performed on a cylindrical sputtering device with a four-turn Cu high-frequency coil installed. The control mesh grid is located directly above the sample specimen. By comparing the deposition between a sample with Cu ions admitted and a sample with Cu ions repelled, the ionization fraction in the plasma is determined to be around 65%.

An *in situ* method for determining the flux ionization fraction requires a gridded energy analyzer (GEA) and a quartz crystal microbalance (QCM). The GEA is located above the QCM and is biased at a potential either to admit or to repel the ions in the plasma. This technique, which we employ, has been previously investigated by Rossnagel and Hopwood.[8,9] When the grids are biased negatively, both ions and neutrals produced in the system arrive at the QCM. When the grids are biased positively, higher than the plasma potential, only the neutrals reach the QCM.[8] These data are used to determine the ionization fraction of the metal flux received at the QCM.

One limitation of the Rossnagel–Hopwood setup is that their QCM is maintained at ground potential. Keeping the

Downloaded 13 Dec 2012 to 130.126.32.13. Redistribution subject to AIP license or copyright; see http://rsi.aip.org/about/rights_and_permissions

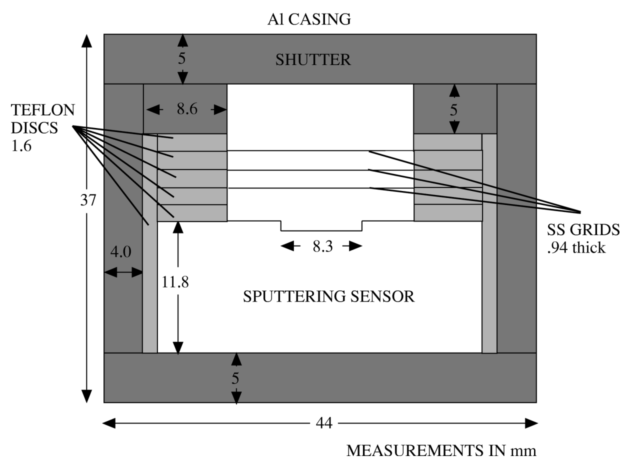

FIG. 1. Schematic of the GEA and QCM. The hollow aluminum cylinder has an inner diameter of 3.4 cm and an outer diameter of 4.4 cm. This piece also has a removable bottom disc to allow the grids and QCM to be placed and secured in the aluminum casing.

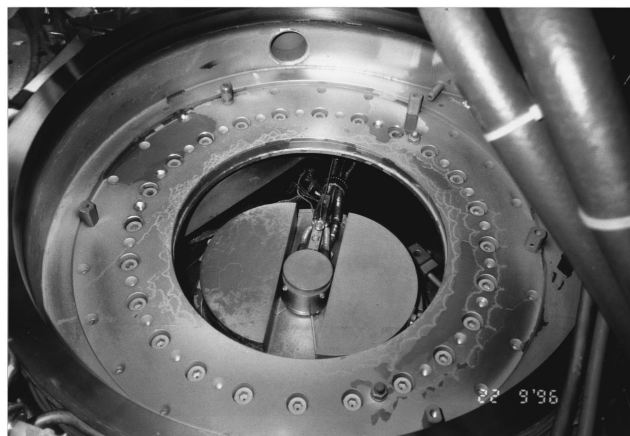

FIG. 2. Diagnostic embedded in slot in the substrate holder.

QCM grounded has the potential of repelling some of the ions even if the grids are biased negatively. Another difficulty is that variations in the substrate potential are not mirrored by the QCM. During some portions of an rf cycle some ions may not be energetic enough to reach the QCM, thereby producing an error in the ionization fraction measurements. The diagnostic described in this paper maintains the QCM at the potential of the substrate, avoiding this difficulty.

A problem with the grids only being effective at low plasma densities is discussed by Rossnagel and Hopwood.[9] In their system, the plasma penetrates the grids once the radio-frequency (rf) power exceeds 500 W and the ion density exceeds 3×10^{11} cm^{-3}. In their experiments the grids are located about 25 mm below the rf coil. Our diagnostic is located 75 mm below the coil and the space between grid wires is 6–12 Debye lengths. Since the sheath formed around each wire is about 4 Debye lengths thick,[10] the sheaths surrounding the grid wires overlap sufficiently to screen the plasma out from the diagnostic.

II. APPARATUS

Figure 1 shows the diagnostic. A GEA consisting of three grids rests below a shutter and is positioned directly above a QCM. Each grid consists of a mesh of 0.094 $\pm$0.004-mm-diam stainless steel wire and has 52.7$\pm$2.1% open area. The open space between the wires is 0.25$\pm$0.01 mm. At a deposition rate of 4 Å/s at a dc power of 2 kW and a pressure of 35 mTorr, the magnetron would have to run constantly for over 2 h with all of the Al flux sticking to the grid to decrease the distance between the grid wires by 1% and the area by 2%. So far no difference in the grid transparency has been measured.

Each grid is also mounted on a 0.79$\pm$0.04-mm-thick teflon disk which has an inner radius of 11$\pm$1 mm and an outer radius of 16$\pm$1 mm. The teflon disks provide a sturdy structure for the grids while insulating the grids from each other. Each grid can be biased independently of the others and their currents can be measured separately.

The diagnostic is operated with a different number of grids depending on the needs of the experiment. For instance, to determine the metal flux ionization fraction, one grid is used. Since each grid attenuates 47.3$\pm$1.9% of the incident flux, having only one grid in the diagnostic allows for screening the ions while producing a strong signal on the QCM.

The water-cooled Leybold–Inficon QCM is in electrical contact with the backplane, and they both are electrically isolated from the rest of the system. Therefore, the QCM, its casing, and the backplane can all be biased at the same potential. The QCM in-vacuum power cable travels from the sputtering sensor through a rf-shielded braid to an electrical feedthrough to prevent rf pickup. A LabVIEW program was written to produce a real-time plot of the total deposition versus time using QCM data. The slope of this plot is the deposition rate.

As seen in Figure 1, a specially designed aluminum casing houses the GEA and QCM. At the top of the casing is a shutter which is connected to the casing by two springs. The shutter is attached to a rotary motion feedthrough which pulls the shutter along a track in the aluminum casing arm to expose the diagnostic *in situ*. The shutter protects the diagnostic from the initial sputter cleaning and also prevents unwanted deposition from clogging the grids when the diagnostic is not in use. The diagnostic is embedded in a slot in the substrate plane (see Figure 2) and is mounted on a linear motion feedthrough which allows the diagnostic to move across the substrate to measure the uniformity of the deposition and the uniformity of the ionization.

To allow the movement of the diagnostic, the substrate holder has been lowered from its normal position in the Materials Research Corporation Galaxy Tool. Two aluminum half-moon shaped ''D's'' with a radius of 7.6$\pm$0.4 cm are placed on the sides of the diagnostic. To minimize interference with the plasma, the top of the diagnostic casing is flush with the top of the ''D's'' and fits snuggly between them.

The built-up substrate holder is located 166$\pm$10 mm below the target but can be moved closer. The rf coils which ionize the Al ejected from the target surface are located between the substrate and target (see Figure 3). The specifics of the coil design and the effects of pressure and input power

Downloaded 13 Dec 2012 to 130.126.32.13. Redistribution subject to AIP license or copyright; see http://rsi.aip.org/about/rights_and_permissions

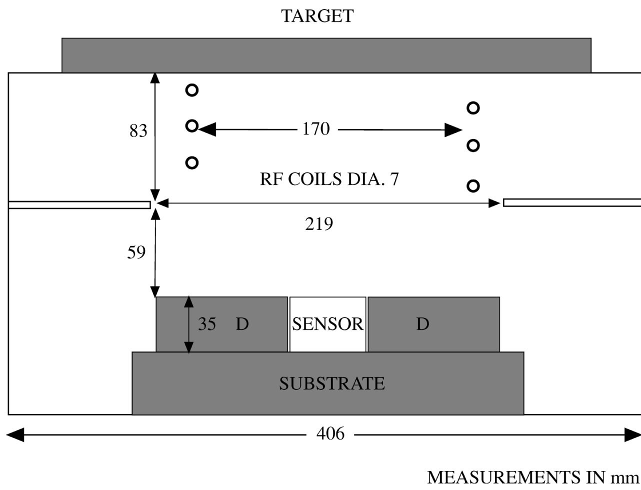

FIG. 3. Schematic of magnetron sputtering machine.

changes on the performance of the magnetron sputtering device are discussed by Hayden *et al.*[11]

III. CALIBRATION

Two different calibrations were performed. The first determined the correlation between the deposition rate on the substrate and on the sensor. The second entailed characterizing the dc magnetron plasma system before ionizing any Al sputter flux.

In a QCM, when a known voltage is applied across a piezoelectric crystal, the crystal resonates at a known frequency. After mass is added to the resonating crystal, the frequency at which the crystal vibrates is decreased. The magnitude of the change in frequency is proportional to the thickness of the deposited layer.

Our QCM measurement has a resolution of $\pm$ 0.1Å if no rf is applied. The addition of rf decreases the resolution to $\pm$0.3 Å, because of a small amount of rf noise that interferes with the reading. The top of the diagnostic casing is even with the substrate plane. The crystal itself is lower, and therefore does not receive the same flux as the substrate. At higher pressure scattering occurs, decreasing the flux further. The fraction of flux that reaches the diagnostic has been determined empirically and is referred to as the geometric factor, G, which is a function of pressure. Taking into account the geometric factor and the grid transparency, the sensor deposition rate is given by

$$R_{\mathrm{sensor}}=(R_{\mathrm{substrate}})(G)(T_g)^n, \tag{1}$$

where R_{sensor} is the deposition rate at the sensor, $R_{\mathrm{substrate}}$ is the deposition rate at the substrate, T_g is the grid transparency, and n is the number of grids in the diagnostic.

With no bias applied to the substrate or sensor, several tests are performed to measure G. Since no rf is introduced during these experiments, all of the Al flux is assumed to be neutral atoms. First, all of the grids are removed from the diagnostic so that only the sputtering sensor remains in the aluminum casing. By comparing the deposition on the sensor to the deposition on the substrate, the effect on the deposition due to geometry and scattering in the gas phase can be determined. A line is drawn across a glass slide using a 3M (TM) nonpermanent medium-point felt-tip pen. The marked glass slide is placed on the substrate holder and sputtered onto while the sensor reads the deposition on the crystal. After an estimated 10 kÅ is deposited, the glass slide is removed and placed in an ultrasonic de-ionized water bath for about 2 min. This process lifts off the marker line along with the aluminum deposited on top of it. The deposition is then measured with a Dektak^{3}ST profilometer to an accuracy of $\pm 5\%$. Comparing the deposition rate measured by the QCM and by the profilometer gives a value of $G=0.215 \pm 0.011$ at 3 mTorr, a pressure low enough that scattering is not significant and $G=0.119\pm 0.006$ at 35 mTorr when scattering is significant.

In addition to the experiment, calculations were done to predict the effect of the geometry of the diagnostic casing on the flux received at the sensor. Since the actual sensor lies at the bottom of a cylindrical hole in the diagnostic casing, the sensor surface is shadowed by the casing walls and is partially shielded from the plasma above. The results of the calculations can be generalized to the filling of trenches and vias of varying aspect ratios. In both calculations collisions within the diagnostic are ignored.

The first calculation assumes an isotropic flux of particles in the region of the sensor. This calculation should correspond to the high pressure case where scattering in the chamber is significant. The flux to a point on the sensor surface relative to the top of the diagnostic can then be calculated by comparing the solid angle encompassed by the visible portion of the plasma. The top surface of the diagnostic sees an entire hemisphere of plasma, for a solid angle of 2π steradians, but the center of the sensor surface sees a cone of height l and width $w=2R$, for a solid angle of only

$$\int_0^{2\pi}\int_0^{\tan^{-1}(R/l)} \sin\,\theta\, d\theta\, d\phi = 2\pi(1-\cos[\tan^{-1}(R/l)]) = 2\pi\left(1-\frac{l}{\sqrt{l^2+R^2}}\right) \tag{2}$$

steradians. From Figure 1 the height, l, is 15 ± 1 mm and R is 9 ± 1 mm. Thus at the center of the sensor surface the flux is only 14.25% that of the top surface.

To calculate the exact decrease in flux analytically at an off-center point on the sensor surface requires integrating over the disks in both the sensor and subtrate planes. The factor, G, by which the flux is decreased is:

$$G=\int_0^R\int_0^{2\pi}\int_0^R\int_0^{2\pi}\frac{\sqrt{r_t^2-2r_t r_b\cos\,\theta_b+r_b^2}}{(l^2+r_t^2-2r_t r_b\cos\,\theta_b+r_b^2)^{3/2}} \times r_t d\theta_t dr_t r_b d\theta_b dr_b, \tag{3}$$

where (r_t,θ_t) is a point in cylindrical coordinates on the top surface of the hole and (r_b,θ_b) is a point in cylindrical coordinates on the bottom surface of the hole. This integral was calculated using a Monte Carlo technique.

A similar simulation was also done for an infinitely long trench of rectangular cross section with height l and width w. In addition to the calculations using an isotropic flux distribution, a second set of calculations using a cosine flux dis-

Downloaded 13 Dec 2012 to 130.126.32.13. Redistribution subject to AIP license or copyright; see http://rsi.aip.org/about/rights_and_permissions

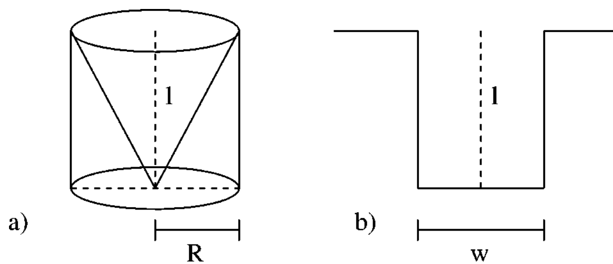

FIG. 4. Geometry of (a) cylindrical hole and (b) rectangular trench.

tribution, which corresponds to the distribution of the sputter flux as it leaves the sputter target, was completed. This distribution should comparatively match an experiment done at low pressure where little scattering is expected. The two geometries are shown in Figure 4.

Figure 5 shows G as a function of aspect ratio (l/w) for both a hole and a trench for both distributions, along with our experimentally measured data. Note that the simple analytic result of 14.25% at the center compares favorably to an aspect ratio of 15/18 (which the diagnostic has). The two experimental points, shown as triangles, indicate that for our system, the flux factor is $0.215\pm.010$ at low pressure (3 mTorr) and $0.119\pm.006$ at high pressure (35 mTorr). These two data points perfectly match the cosine and isotropic distribution data, respectively. In all cases, the uncertainty in the data is less than the size of the data point.

These results are consistent because at 3 mTorr, the sensor is about two mean free paths from the target, while at 35 mTorr it is nearly 20 mean free paths from the target, where the mean free path refers to an Al atom through argon gas. Collisions between the sputter flux and the neutral gas are strongly forward peaked, so two collisions are not enough to destroy the cosine distribution of sputter flux at 3 mTorr. However, at 35 mTorr the sputter flux has so many collisions that the velocities are randomized, resulting in an isotropic distribution to the sensor.

Note that for both geometries and distributions, as the aspect ratio goes to 0, the flux factor approaches 1, indicating that the flux on the bottom surface is equal to that on the top

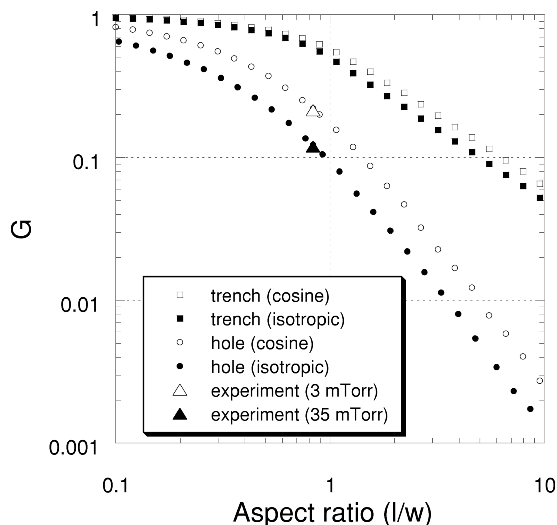

FIG. 5. Flux factor as a function of aspect ratio.

TABLE I. Effects of grids on deposition rates measured on sensor.

Grids No.	Substrate (Å/s)	Sensor (Å/s)	Theory (Å/s)
0	33.5±1.7	7.20±0.04	7.37±0.01
1	32.7±1.6	3.10±0.02	3.79±0.01
2	32.9±1.6	1.90±0.01	2.01±0.01
3	32.0±1.7	1.10±0.01	1.03±0.01

surface, as expected. As the aspect ratio (for either distribution) approaches infinity, the flux factor for the hole is proportional to $(l/w)^{-2}$ and that for the trench is proportional to $(l/w)^{-1}$, which is evident as the plots approach appropriately sloped straight lines for high aspect ratios on the log-log scale.

One implication of these geometric calculations is that even a small increase in the ionization fraction in the plasma can result in a large increase in flux to the surface feature, with a large fraction of that flux being in the form of ions. This increase occurs because ions fall through a sizable voltage drop at surfaces, accelerating them to a near-normal velocity distribution. Therefore the ion flux to the bottom of a surface feature is the same as the ion flux to the surface above it. Effectively, $G_{\text{ion}}=1$.

For instance, the bottom of a hole with an aspect ratio of 4 receives less than 1% of the neutral flux that the surface above it receives. If only 10% of the incoming flux were ionized (all of which makes it to the bottom of the hole), then the total flux to the bottom of the hole would be increased by a factor of 10.9, 91.7% of which would be made up of ions.

In the case of a trench, the difference is less dramatic but still significant. Again using an aspect ratio of 4, ionizing 10% of the incoming flux results in a doubling of total flux, with half of it being in the form of ions.

For the final calibration, done at 3 mTorr, grids are placed in the diagnostic above the sputtering sensor. Each grid has a transparency of $52.7\pm2.1\%$. So using Equation (1), with one, two, and three grids the sensor deposition rate is expected to be 6.4%, 3.4%, and 1.8% of the substrate deposition rate, respectively. Table I gives the actual deposition rates measured at the sensor and substrate as well as the deposition rates predicted by theory.

IV. RESULTS

A. Deposition rate

The deposition incident on the substrate differs depending on the pressure in the sputtering chamber and the power at which the magnetron is run. The deposition rate decreases as the chamber pressure increases, as expected,[5] so experiments are run at high and low pressures to characterize the deposition rates. One grid is used in the diagnostic. The grid and the substrate are biased at −30 V. At 3 mTorr, a typical pressure for conventional magnetron sputtering, and at 35 mTorr, a pressure often used for ionized PVD experiments, the deposition rates have been measured at magnetron powers of 2, 4, 6, and 8 kW (see Figure 6).

Downloaded 13 Dec 2012 to 130.126.32.13. Redistribution subject to AIP license or copyright; see http://rsi.aip.org/about/rights_and_permissions

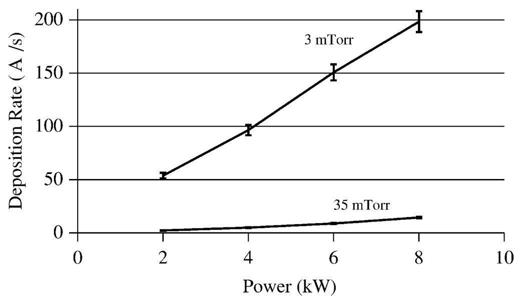

FIG. 6. Deposition rate on substrate vs power at 3 mTorr and 35 mTorr.

B. Collected current

To ionize the Al atoms, an rf coil is introduced into the magnetron system. The effects of the rf power are seen directly on the grid currents. Several experiments are run with all three grids in the diagnostic and with the substrate maintained at −30 V.

First, biases of −30±1 V, 20±1 V, and −30±1 V are applied to grid 1, grid 2, and grid 3 respectively, and a −30 V bias on the substrate and QCM. The magnetron is run at a dc power of 2 kW and a pressure of 35 mTorr. Without introducing any rf power, the current on grid 1 is 65.2±5.2 μA, on grid 2 is −22.5±1.8 μA, and on grid 3 is 3.7±0.3 μA. Holding all other parameters constant and introducing 310±5 W of rf power, the currents are 0.438±0.035 mA on grid 1, −0.059±0.005 mA on grid 2, and 0.015±0.001 mA on grid 3. The currents on grid 1 and grid 3 increase their values by over four times with the introduction of rf power, thus the rf coil is clearly ionizing particles in the chamber. The current on grid 2 increases only by 2.5 times. Even though the rf power creates as many electrons as ions in the chamber, these electrons are not very energetic. So only a few of the electrons have the energy to pass through the −30 V bias of grid 1 and get collected on grid 2.

TABLE II. Effects of altering grid 3 bias on grid currents.

Grid 1		Grid 2		Grid 3	
Voltage (V)	Current (mA)	Voltage (V)	Current (mA)	Voltage (V)	Current (mA)
−30±1	0.40±0.03	20±1	−15.0±1.2	−7±1	0.03±0.01
−30±1	0.38±0.03	20±1	−16.4±1.3	−30±1	0.08±0.01
−30±1	0.41±0.03	20±1	−14.9±1.2	−46±1	0.08±0.01

Table II gives an example of the effects of changing the grid 3 bias. The current on each grid is shown for the different biases. These data are taken with a dc magnetron power of 2 kW, a net rf power of 310±5 W, and a pressure of 35 mTorr. Each individual grid follows the expected trend of having an increasing current if its bias is made more negative and having a decreasing current if its bias is made more positive.

The change in the current on grid 3, seen in Table II, demonstrates the effects of secondary electron emission. The secondary electrons produced on grid 1 are born at an energy of −30 V. Some of these secondary electrons produced on grid 1 are accelerated to grid 2 where most of them are collected. However, a few of the secondary electrons pass through grid 2 and slow down as they reach grid 3. When the bias on grid 3 is less than −30 V, the electrons are energetic enough to reach grid 2 and be collected. In Table II, when the bias on grid 3 is −7±1 V, the current on grid 3, 0.03 ±0.01 mA, is the sum of the current from the ions and the current from the electrons. When the bias on grid 3 is greater than −30 V, all of the secondary electrons born on grid 1 are repelled before reaching grid 3. So when the bias on grid 3 is 46±1 V, the current on grid 3, 0.08±0.01 mA, is just the current from the ions. So the secondary electrons from grid 1 cause a change in the current on grid 3 by 0.05±1 mA when grid 3 is maintained at a bias below −30 V.

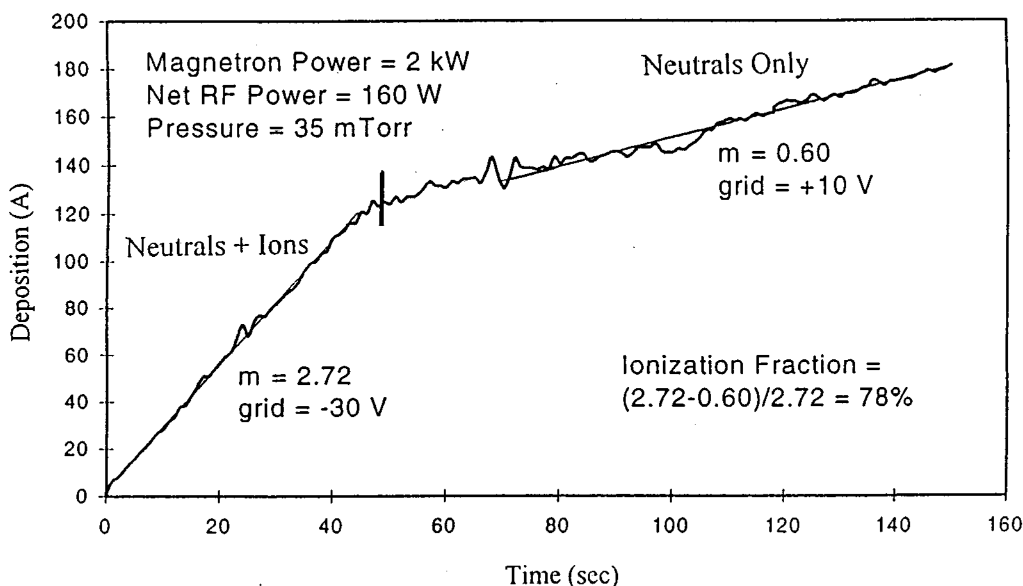

FIG. 7. Deposition vs time graph for determining flux ionization fraction.

Downloaded 13 Dec 2012 to 130.126.32.13. Redistribution subject to AIP license or copyright; see http://rsi.aip.org/about/rights_and_permissions

When the grid is biased to admit ions, the QCM measures the total flux, ψ_{tot}, where

$$\psi_{tot} = \psi_N + \psi_I . \tag{4}$$

Using the QCM and the GEA, the metal flux ionization fraction is measured. The substrate, sensor, and grids 1 and 3 are maintained at −30 V during the experiment. When the grid 2 bias exceeds the plasma potential, the ions are repelled and only the neutral flux reaches the QCM. From the total flux and the neutral flux, the metal flux ionization fraction is calculated:

$$\text{metal flux ionization fraction} = \frac{\psi_{tot} - \psi_N}{\psi_{tot}} . \tag{5}$$

This test is run at 35 mTorr with a dc magnetron power of 2 kW and a net rf power of 420±10 W.

The total flux is measured with grid 2 biased at −30 V to admit the Al ions. Then the neutral flux is measured with the grid biased to repel the Al ions at 20 V, which is higher than the plasma potential at these powers and pressure.

Figure 7 shows the deposition versus time for a typical run. These data were collected during the experiment using LabVIEW software. The initial part of the curve shows the accumulation of metal when both the neutrals and the ions are incident on the QCM. At 40 s the 20 V bias is placed on the grid. From 40 s on, the graph shows the accumulation of metal caused only by Al neutrals.

To determine the deposition rates of the total flux and the neutral flux, lines are fitted to the two different sets of data. The first line is fit to the data for the total flux over the first 40 s. The slope of this line, 2.72±0.03 is the deposition rate of the total flux in Å/s. The second line is fit to the data for the neutral flux from 40 to 150 s. The slope of this line, 0.60±0.04, is the deposition rate of the neutral flux. These deposition rates are not calibrated for the substrate surface, but that calibration is unnecessary for calculating the metal flux ionization fraction reaching the bottom of the diagnostic. Using Equation (5), the ionization fraction of the depositing aluminum is 78±5%.

ACKNOWLEDGMENTS

This research was performed under appointment to the Nuclear Engineering/Health Physics Fellowship program administered by Oak Ridge Institute for Science and Education for the U.S. Department of Energy, and by funding and equipment from Materials Research Corporation. D. R. Juliano was supported by the Fannie and John Hertz Foundation during the period this work was performed.

[1] *Thin Film Processes,* edited by J. L. Vossen and W. Kern (Academic, New York, 1978).
[2] *VLSI Technology,* 2nd ed., edited by S. M. Sze (McGraw-Hill, New York, 1988).
[3] *National Technology Roadmap for Semiconductors* (Semiconductor Industry Association, San Jose, CA, 1994).
[4] S. M. Rossnagle, D. Mikalsen, H. Kinoshita, and J. J. Cuomo, J. Vac. Sci. Technol. A **9**, 261 (1991).
[5] P. F. Cheng, S. M. Rossnagel, and D. N. Ruzic, J. Vac. Sci. Technol. B **13**, 203 (1995).
[6] W. M. Holber, J. S. Logan, H. J. Grabarz, J. T. C. Yeh, J. B. O. Caughman, A. Sugarman, and F. E. Turner, J. Vac. Sci. Technol. A **11**, 2903 (1993).
[7] M. Yamashita, J. Vac. Sci. Technol. A **7**, 151 (1989).
[8] S. M. Rossnagel and J. Hopwood, Appl. Phys. Lett. **63**, 3285 (1993).
[9] S. M. Rossnagel and J. Hopwood, J. Vac. Sci. Technol. B **12**, 449 (1994).
[10] D. N. Ruzic, *Electric Probes for Low Temperature Plasmas* (AVS Monograph Series, New York, 1994).
[11] D. B. Hayden, D. N. Ruzic, K. M. Green, D. R. Juliano, C. A. Weiss, K. A. Ashtiani, and T. J. Licata, J. Vac. Sci. Technol. A (submitted).

Downloaded 13 Dec 2012 to 130.126.32.13. Redistribution subject to AIP license or copyright; see http://rsi.aip.org/about/rights_and_permissions